Climate Physics and Atmospheric Science: Scientific Insights and Societal Challenges 1–2 (2026) 100006

Contents lists available at ScienceDirect

Climate Physics and Atmospheric Science: Scientific Insights and Societal Challenges

journal homepage: www.elsevier.com/locate/cpas

Full Length Article

Aerosol loading, hotspot contributions, and climatic interactions across West African climate zones and adjacent regions of Chad and Cameroon

Oluseye David Dare[a,b], Modupe E. Sanyaolu[a,*], Ayodele O. Soge[a], Alexander A. Willoughby[a]

[a] Department of Physical Sciences, Faculty of Natural Sciences, Redeemer's University, Ede, Osun State, Nigeria
[b] Department of Physical Sciences, Faculty of Pure and Applied Sciences, Precious Cornerstone University, Ibadan, Oyo State, Nigeria

ARTICLE INFO

Keywords:
Aerosol optical depth (AOD)
Biomass-burning
Dust
Percentage relative AOD (% RAOD)
West Africa (WA)

ABSTRACT

This study evaluates aerosol concentration variations (ACV) and their associations with climatic parameters across five West African zones and Central Africa, using 16 years (2008–2023) of satellite data from NASA's Giovanni platform (MODIS, MERRA-2, AIRS, GPCPMON, GLDAS, and MISR). Central Africa were included because of their geographical continuity with the West Africa. Aerosol metrics (Aerosol Optical Depth [AOD], fine Particulate Matter [$PM_{2.5}$], Black Carbon [BC], Organic Carbon [OC]) and climatic variables were analyzed using correlation heatmaps, scatter plots, and multiple linear regression. Results show a strong positive correlation between AOD temperature (up to r = 0.74 in the Sudanian zone) and negative associations with precipitation (-0.67 in Sudanian; -0.63 in Sahara). Seasonal peaks varied by zone: Dust-driven in the arid north (Araouane, Mali: 0.74 in June; Fada N'gourma, Burkina Faso: 0.80 in March) and biomass-burning February-driven in the Sudanian belt (Kano, Nigeria: 1.35 in February), and urban-industrial in the humid south (Lagos, Nigeria: 1.07 in). Chad, Abeche and Moussoro show late dry-season peaks (0.66–0.76), while Cameroon (Douala, Limbe, Buea) exhibits moderate but persistent AOD (~0.87). A regional maximum occurred in 2015, with zonal annual mean of 0.4412 in the Sahara, 0.4921 in the Sahel, 0.6134 in the Sudanian, 0.5510 in the Guinean, and 0.5847 in the Coastal zones. %RAOD identified dominant hotspots, including Araouane (17.11% in 2018), Fada N'gourma (18.48% in 2020), Kano (16.48% in 2020), and Lagos (17.06% in 2009; 16.66% in 2023). These patterns confirm a north-south aerosol gradient consistent across West Africa and adjacent regions.

1. Introduction

Atmospheric aerosols are tiny substances other than pure water, present in solid and/or liquid phases that remain suspended in air with a minimum stability or lifetime of about one hour [1]. They can originate from either natural or anthropogenic sources, and play important roles in regulating climate by influencing temperature, relative humidity, precipitation, wind speed, and other parameters [2,3]. Depending on their atmospheric residence, aerosols affect climate either directly through scattering or by absorbing shortwave

* Corresponding author.
E-mail addresses: dare15905@run.edu.ng (O.D. Dare), sanyaolum@run.edu.ng (M.E. Sanyaolu), sogea@run.edu.ng (A.O. Soge), willoughbya@run.edu.ng (A.A. Willoughby).

https://doi.org/10.1016/j.cpas.2026.100006
Received 30 November 2025; Received in revised form 27 March 2026; Accepted 9 April 2026
Available online 12 April 2026

radiation [4,5]. Dust, smoke, and industrial haze are mainly found in the troposphere; volcanic sulfuric acid aerosols occur in the stratosphere, while the planetary boundary layer hosts the primary sources and sinks of atmospheric aerosols [6,7].

The climatic role of aerosols is expressed through three pathways: the direct effect, where aerosols scatter solar radiation back to space leading to cooling or absorb it causing atmospheric warming; the semi-direct effect, in which absorption leads to cloud droplet evaporation and suppression of cloud formation; and the indirect effect, where aerosols act as CCN, altering cloud microphysics and lifetime [8]. Haywood et al. [9], for example, estimated a mineral dust radiative forcing between −60 and −35 Wm^{-2} over Cape Verde, highlighting their strong cooling influence. The IPCC [10] emphasized that clouds and aerosols still pose the greatest uncertainty in quantifying the Earth's energy budget.

The Aerosol Optical Depth (AOD) measures the extent of light attenuation by aerosols along a vertical atmospheric column. Most aerosols, such as nitrates, sulfates, organic carbon, and mineral dust, scatter radiation, whereas black carbon and biomass-burning aerosols are strong absorbers [11–13]. According to Zhang et al. [7], the magnitude of AOD indicates its atmospheric influence: values below 0.1 present clear skies, while AOD values close to 1 indicate a dusty atmosphere with poor visibility [6]. Aerosols in Sub-Saharan Africa frequently act as cloud condensation nuclei (CCN), reducing cloud droplet size, suppressing drizzle, and modifying cloud lifetime [14–17]. They are also mobilized during squall line events, which enhance dust entrainment into the atmosphere [18].

Dust aerosols, in particular, have been widely recognized as major modulators of Earth's climate system. Engelstaedter and Washington [19], De Longueville *et al.* [20], and Wells et al. [21] affirmed the importance of dust emissions from desert regions in altering climate and environment, with West Africa and the Bodélé Depression in Chad identified as the largest global sources. The West African region also experiences the prevailing northeasterly wind regime known as the Harmattan between November and March, which transports large quantities of mineral dust across the region [22–24].

More recent studies have sought to refine this understanding in West Africa. Akinyoola *et al.* [25], using infrared forcing (IRF) datasets from the Copernicus Atmosphere Monitoring Service (CAMS), quantified aerosol radiative forcing and found a positive correlation between IRF and solar radiation absorption. The study further showed that aerosol-radiation interactions (IRFari) enhance regional forcing, contributing to warming and extreme events in West Africa. Similarly, Ochei et al. [8], using 30 years of data from six climate zones, examined biomass burning, carbonaceous aerosols, dust, $PM_{2.5}$, convective precipitation, wind speed, and water vapour. Their analysis revealed seasonal abundance of aerosols during the dry season in rainforest regions and a strong negative correlation between convective precipitation and most aerosol types, except carbonaceous particles. Importantly, water vapour showed the strongest correlations with aerosols, underscoring its role in aerosol-climate interactions. However, despite these efforts, there remains a limited understanding of the spatial variability of aerosol hotspots and their statistical relationships with climatic parameters across the different West African climate zones, including some locations in Chad and Cameroon. This highlights a major research gap [21]. This study aims to address this gap by providing the broader effects of aerosols on air pollution, their hotspot contributions, and climate in West Africa, Chad, and Cameroon.

2. Study area

Although the study focuses mainly on West African climate zones, selected locations in Chad and Cameroon were also included due to their geographical proximity and shared climatic characteristics with the Sahelian and Coastal zones of West Africa. This enables a more regionally consistent assessment of aerosol variability across contiguous climatic systems. West Africa is roughly situated between latitudes 2 °N and 25 °N, and longitudes 25 °W and 25 °E, covering an estimated area of $6,140,000\ km^2 (2,372,119\ mi^2)$ [8].

The Sahara zone represents a hyper-arid desert environment mostly affected by intense dust storms that significantly increase regional and transboundary aerosol levels. Immediately south of the Sahara, the Sahel zone is a semi-arid transition zone where seasonal biomass burning is common, especially during the dry season. Further south, the Sudanian zone functions as a transitional savanna, influenced by both dust transport from the north and rising human emissions from urban centers and agriculture. The Guinean zone is a humid savanna with high biomass burning and agricultural activity, both of which greatly contribute to aerosol emissions during dry months. Lastly, the Coastal zone is a wet tropical belt where urban-industrial activity, dense populations, and energy consumption heighten air pollution and aerosol concentrations. The locations in Chad are within the Sahel zone, while those in Cameroon are in the Coastal zone. Fig. 1 represents the study area, including the five climate zones (Sahara, Sahel, Sudanian, Guinean, and Coastal) with the specific locations in Cameroon and Chad, as well as grid points representing selected sites across the fifteen African countries under study.

The West African region spans from the arid Sahara Desert located in the north to the Coastal Rainforest in the south, with diverse and ecologically rich areas. There are sixteen countries within the zone, namely: Benin, Burkina Faso, Cape Verde, Ivory Coast, the Gambia, Ghana, Guinea, Guinea-Bissau, Liberia, Mali, Mauritania, Niger, Nigeria, Senegal, Sierra Leone, and Togo. Chad and Cameroon are the two Central African countries that share borders directly with West Africa. The various climate zones, countries considered in each zone, the three stations selected from each country, their coordinates, the mean AOD (Climax and Trough), and the corresponding months are given in Table 1.

3. Data and methodology

The datasets employed in this study were obtained from the Goddard Earth Sciences Data and Information Services Centre (GEC DISC) Giovanni system, an advanced online platform developed by NASA for the retrieval, visualization, and analysis of atmospheric and climate-related datasets. Giovanni provides access to high-resolution, satellite-derived environmental variables and has been widely recognized as a reliable tool for atmospheric and climate research. In this study, Giovanni was leveraged to evaluate aerosol

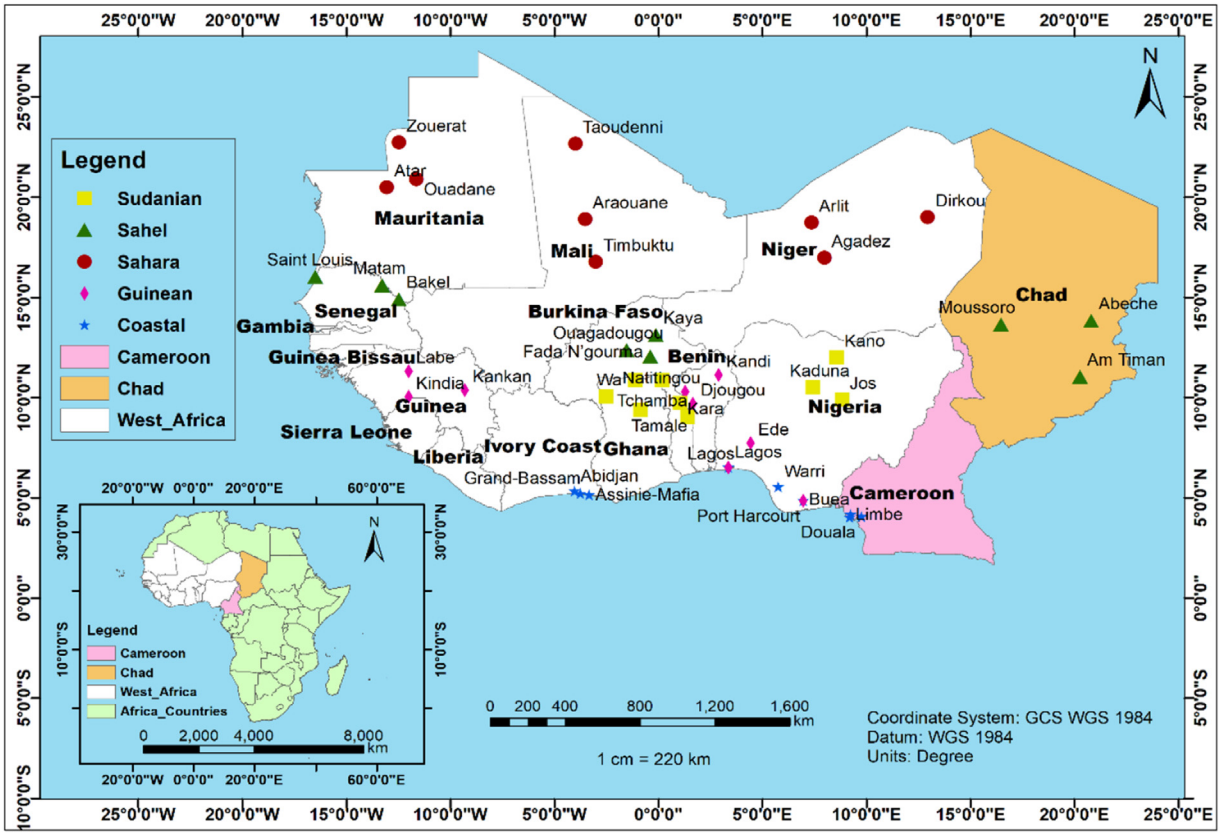

Fig. 1. Map of West Africa (white), and part of Central Africa showing the five climate zones (Sahara, Sahel, Sudanian, Guinean, and Coastal), locations in Chad (Abeche, Am Timan, Moussoro) and Cameroon (Buea, Douala, Limbe), with grid points of selected locations used in the analysis.

concentration variations (ACV), hotspot contributions, and their impacts on climatic parameters across five West African climate zones and part of Central Africa, namely, Cameroon and Chad.

Time series, Area-Average aerosol and meteorological data were derived from NASA's Moderate Resolution Imaging Spectroradiometer (MODIS), Modern-Era Retrospective Analysis for Research and Applications, version 2 (MERRA-2), Atmospheric Infrared Sounder (AIRS), and Multi-angle Imaging Spectroradiometer (MISR) instruments. Specifically, AOD data at wavelength 550 nm from MISR (2008 – 2017) and MODIS-Terra (2018 – 2023) with spatial resolution 1°, were employed as an important indicator of columnar aerosol load. Additional aerosol variables included monthly $PM_{2.5}$, BC, and OC data from MERRA-2 (Reanalysis data) with spatial resolution 0.5° x 0.625° To assess the interactions between aerosols and climate, corresponding meteorological parameters – air temperature from GLDAS_NOAH10_M (1°), precipitation from AIRS/SSMI combined product (sat. gauge; 0.5°), relative humidity from AIRS-only retrievals (1°), precipitable water vapour from MODIS-Aqua (sat. retrieval; 1°), and wind speed from MERRA-2 (reanalysis; 0.5° x 0.625°) were also retrieved from the same platform. All data were obtained from Giovanni-accessible datasets and compiled at a monthly temporal resolution for a period of sixteen years (2008–2023), enabling robust analysis of both seasonal patterns and long-term trends.

The study domain was defined by the five major climate zones in West Africa: the Sahara, the Sahel, the Sudanian, the Guinean, and the Coastal regions. Within each zone, three countries were selected based on data availability, and three locations within each country were further chosen to ensure spatial representativeness. This design resulted in a total of 45 stations distributed across 15 countries. Additional locations were included in Chad and Cameroon to extend the spatial coverage into adjacent regions having similar climatic regimes. This enables a more comprehensive assessment of aerosol variability across the West African – Central African transition zone. The selected locations and their respective zones are explicitly illustrated in Fig. 1.

Before analysis, the raw datasets underwent a series of preprocessing steps. The very few missing gaps in AOD data were imputed using mean interpolation. The preprocessed data were subsequently exported for analysis in Python, where statistical modeling and geospatial interpolation techniques were applied. Analysis procedures included: (i) the determination of seasonal cycles of aerosols and AOD; (ii) long-term trend analysis of aerosol concentrations; (iii) scatter matrix analysis to examine pairwise relationships between aerosols and climatic parameters; and (iv) computation of correlation coefficients, supported by the visualization of correlation heatmaps, to quantify the strength and direction of associations. Collectively, these methods enabled a comprehensive spatiotemporal assessment of aerosol-climate interactions across the diverse climatic regimes of West Africa.

Table 1
Showing each climate zone with the countries considered, every location from each country, the coordinates, the mean AOD (Climax and Trough), and the months of their occurrence.

Climate Zone	Country Selected	Location Selected	Coordinate	Mean AOD (Climax)	Month	Mean AOD (Trough)	Month
Sahara	Niger	Agadez	16.97°N, 7.99°E	0.59	June	0.24	Dec
		Arlit	18.73°N, 7.37°E	0.63	June	0.12	Dec
		Dirkou	19.01°N , 12.96°E	0.67	June	0.37	Nov
	Mali	Timbuktu	16.77°N , 3.00°W	0.63	June	0.27	Nov
		Taoudenni	22.67°N , 3.98°W	0.62	July	0.13	Nov
		Araouane	18.90°N , 3.50°W	0.74	June	0.42	Nov
	Mauritania	Atar	20.50°N , 13.05°W	0.53	July	0.21	Nov
		Ouadane	20.90°N , 11.62°W	0.55	July	0.27	Nov
		Zouerat	22.74°N , 12.47°W	0.53	July	0.18	Nov
Sahel	Burkina Faso	Ouagadougou	12.37°N , 1.52°W	0.66	Mar	0.23	Aug
		Kaya	13.12°N , 0.10°W	0.76	Mar	0.23	Aug
		Fada N'gourma	12.06°N , 0.37°W	0.80	Mar	0.28	Aug
	Chad	Abeche	13.83°N, 20.83°E	0.66	April	0.17	Dec
		Moussoro	13.65°N, 16.49°E	0.76	April	0.23	Nov
		Am Timan	11.04°N, 20.28°E	0.50	Mar	0.21	Nov
				0.50	June		
	Senegal	Saint Louis	16.03°N , 16.48 °W	0.45	June	0.20	Nov
		Matam	15.60 °N, 13.26 °W	0.58	May	0.26	Nov
		Bakel	14.90 °N, 12.46 °W	0.57	May	0.24	Aug
Sudanian	Nigeria	Kano	12.00 °N, 8.59 °E	1.07	Feb	0.35	Aug
		Kaduna	10.51 °N, 7.44 °E	0.92	Feb	0.34	Nov
		Jos	9.89 °N, 8.85 °E	0.78	Feb	0.24	Nov
	Togo	Kara	9.72 °N, 1.06 °E	0.95	Feb	0.35	Sept, Nov
		Tchamba	9.03 °N, 1.41 °E	0.95	Feb	0.35	Sept, Nov
		Dapaong	10.87 °N , 0.20 °E	0.87	Feb	0.27	Sept
	Ghana	Tamale	9.40 °N , 0.85 °W	0.88	Feb	0.34	Sept, Oct
		Navrongo	10.89 °N 1.09 °W	0.77	Feb	0.31	Sept
					Mar		
		Wa	10.06 °N, 2.50 °W	0.66	Feb	0.28	Sept
Guinean	Nigeria	Ede	7.73 °N, 4.44 °E	1.18	Feb	0.40	May –July
		Lagos	6.52 °N, 3.38 °E	1.35	Feb	0.45	June – Oct
		Port Harcourt	4.85 °N, 6.97 °E	1.14	Feb	0.28	June – Oct
	Benin	Djougou	9.70 °N, 1.67 °E	0.96	Feb	0.35	Sept. Nov
		Natitingou	10.30 °N, 1.38 °E	0.86	Feb	0.34	Sept
		Kandi	11.13 °N, 2.93 °E	0.77	Mar	0.28	Aug
	Guinea	Kankan	10.38 °N, 9.30 °W	0.66	Feb	0.28	Nov
		Labe	11.32 °N, 12.29 °W	0.58	April	0.25	Nov
		Kindia	10.04 °N, 12.86 °W	0.65	April	0.27	Nov
Coastal	Nigeria	Lagos	6.52 °N, 3.38 °E	1.35	Feb	0.48	June – Oct
		Port Harcourt	4.85 °N, 6.97 °E	1.14	Feb	0.28	June – Oct
		Warri	5.55 °N, 5.77 °E	1.18	Feb	0.55	May – Oct
	Ivory Coast	Abidjan	5.33 °N, 4.02 °W	1.05	Feb	0.35	July – Oct
		Assinie-Mafia	5.14°N , 3.32 °W	1.06	Feb	0.31	May – Oct
		Grand-Bassam	5.21 °N, 3.74 °W	1.06	Feb	0.31	May – Oct
	Cameroun	Douala	4.05 °N, 9.77°E	0.87	Feb	0.34	May, Aug, Oct
		Limbe	4.02 °N, 9.20°E	0.87	Feb	0.34	Aug, Oct
		Buea	4.15 °N, 9.25°E	0.87	Feb	0.34	May, Aug, Oct

The mathematical calculations for the *scatter matrix* were done using Eq. (1)

$$\text{Scatter Matrix (S)} = \left(x_i - \mu\right)(x_i - \mu)^T \tag{1}$$

Where x_i represents the $i-th$ data point (a vector), μ is the mean vector of the data, Σ denotes the summation over all data points, and T denotes the transpose of a matrix/vector.

The Scatter Matrix is closely related to the covariance matrix, which depicts the scatter matrix scaled by a factor of $\frac{1}{(n-1)}$, where n is the number of data points as expressed in Eq. (2).

$$\text{Covariant Matrix } (\Sigma) = \frac{S}{(n-1)} \tag{2}$$

The correlation matrix is a standardized version of the covariance matrix. It represents the linear relationship between pairs of variables in the datasets. The formula is given by Eq. (3).

$$\text{Correlation Matrix (R)} = \left[r_{ij}\right] \tag{3}$$

Where r_{ij} is the Pearson Correlation Coefficient between variables i and j. Hence,

$$\text{Correlation Coefficient } (r_{ij}) = \frac{\text{Cov}(X_i,\ X_j)}{(\sigma_i * \sigma_j)} \tag{4}$$

Where $\text{Cov}(X_i,\ X_j)$ is the covariance between variables X_i and X_j, σ_i is the standard deviation of X_i, talking about the measure of the dispersion or spread of the value of X_i around its mean (μ_i), mathematically given by Eq. (5)

$$\sigma_i = \sqrt{\frac{1}{n}\sum_{t=1}^{n}\left(X_{i,t} - \mu_i\right)^2} \tag{5}$$

n = number of observations, determined by (16 years × 12 months = 192), $X_{i,t}$ = value of X_i at time t, and μ_i = mean of X_i given by Eq. (6).

$$\mu_i = \frac{1}{n}\sum_{t=1}^{n} X_{i,t} \tag{6}$$

The term $(X_{i,t} - \mu_i)^2$ represents the square deviation from the mean. Also, σ_j is the standard deviation of a climatic parameter X_j expressed as given in Eq. (7).

$$\sigma_j = \sqrt{\frac{1}{n}\sum_{t=1}^{n}\left(X_{j,t} - \mu_j\right)^2} \tag{7}$$

Where σ_j = Standard deviation of variable X_j, n = Number of Observations, $X_{j,t}$ = value of X_j at time t, μ_i = mean of X_i given by Eq. (8).

$$\mu_j = \frac{1}{n}\sum_{t=1}^{n} X_{j,t} \tag{8}$$

The covariant matrix was obtained from the covariance matrix by standardizing each element as given in Eq. (9).

$$R = D\Sigma D \tag{9}$$

Where Σ is the covariance matrix, and D is a diagonal matrix with the inverse standard deviations of the variables on the diagonal.

As a statistical tool for analyzing the relationship between AOD and various climatic parameters across the mentioned climatic zones in West Africa and part of Central Africa, the Multiple Linear Regression (MLR) was used. According to Ran *et al.* [26], the MLR has the advantage of not requiring the details of the classification of internal mixed modes of each aerosol and their corresponding spatial difference. Moreover, the study affirms that the coefficients of MLR are designed to depend on aerosol and the country, and therefore provides additional insight into the relative importance of each aerosol to local $PM_{2.5}$. It also offers clues on observational and simulation bias. The method enables the statistical assessment of relationships between aerosol concentrations and environmental factors, such as air temperature, relative humidity, wind speed, precipitation, and water vapour, over time. The MLR model is given in Eq. (10).

$$Y_{i,t} = \beta_o + \beta_1 X_{1,t} + \beta_2 X_{2,t} + \ldots + \beta_k X_{k,t} + \epsilon_{i,t} \tag{10}$$

where $Y_{i,t}$ are dependent variables; air temperature, humidity, precipitation and so on, $X_{1,t}$, $X_{2,t}$, …, $X_{k,t}$ are independent variables like AOD, $PM_{2.5}$, BC and OC, β_o is the intercept and β_1, β_2, …, β_k are the Regression Coefficient which describes the statistical relationships between of each aerosol type and climatic parameters, $\epsilon_{i,t}$ is the error term which accounts for unexplained variability [27].

In this study, the Multiple Linear Regression (MLR) is used in a supplementary manner to support correlation-based interpretations. It is not used as the primary basis for inference.

The Zonal Annual Mean AOD was determined using Eq. (11) while the percentage relative AOD was calculated using Eq. (12).

$$Zonal\ Annual\ Mean = \frac{\sum_{j=1}^{n} AOD_{j,t}}{n} \tag{11}$$

$$\%RAOD_{i,t} = \left(\frac{AOD_{i,t}}{\sum_{j=1}^{n} AOD_{j,t}}\right) \times 100\% \tag{12}$$

Where: $AOD_{i,t}$ = Annual mean AOD at location i in the year t

$\sum_{j=1}^{n} AOD_{j,t}$ = Sum of annual mean AOD values across all n locations within the same zone z for the year t

$\%RAOD_{i,t}$ = Percentage contribution of location i to the total zonal AOD in the year t n = Number of locations within a zone

It is worth noting that $PM_{2.5}$, Organic Carbon, and Black Carbon were measured in mg/m^2; the unit for precipitation was expressed as mm/day; relative humidity was given as a percentage (%); wind speed was measured in m/s, air temperature in °C; water vapour in cm; and AOD is unitless. This standardization enabled better comparison of these parameters across the various climate zones in West Africa and part of Central Africa, by facilitating an effective comparison of how these zones experience aerosol fallout. It also aided in understanding long-term aerosol deposition, which is essential for a better understanding of environmental changes over time, such as shifts in soil fertility, desertification, and impacts on local climate.

4. Results and discussions

Based on the approaches adopted as discussed in Section 3.0, the correlation heatmaps, the seasonal pattern of aerosols, trends in aerosol concentration over time, scatter matrix of aerosols and environmental factors for the different locations in each climate zone were considered for assessing the impact of aerosol concentration variation on climatic parameters.

4.1. Correlation analysis across zones

The correlation heatmaps (Fig. 2a-e) reveal pronounced spatial contrasts in aerosol loading and its climatic controls across the representative hotspot locations in the five West African climate zones. In the Sahara zone (Araouane, Mali), AOD shows positive correlations with temperature, and water vapour (r = 0.72), precipitation (r = 0.32), and relative humidity (r = 0.25). This suggests that dust loading occasionally coexists with moist air during transitional periods. The weak anti-correlation with wind speed (r = −0.18) suggests that excessively strong winds may disperse rather than concentrate suspended dust, modulating columnar aerosol burden.

In the Sahel location (Kaya, Burkina Faso), AOD correlates positively with temperature (r = 0.12) and negatively with water vapour (r = −0.27), precipitation (r = −0.30), and humidity (r = −0.39), while indicating a positive link with wind speed (r = 0.37). This pattern reflects Harmattan-driven dust uplift under dry, windy, and low-humidity conditions. Similar trends are observed in the Sahelian extension into Chad (Abeche, Moussoro, and Am Timan), with aerosol loading associated with dry conditions, moderate wind influence, and reduced precipitation. This suggests that aerosol variability in Chad is consistent with Harmattan-dust transport and seasonal biomass burning observed across the rest of the Sahel.

The Sudanian zone (Wa, Ghana) portrays similar behavior of negative associations with moisture variables (r = −0.36 to −0.47) and a positive correlation with wind speed (r = 0.46). This emphasizes that biomass-burning and dust infiltration intensify aerosol loading during the late dry season. Toward the humid south, aerosol hotspots transition from natural dominance to anthropogenic. In Ede, Nigeria (Guinean zone), AOD correlates strongly and negatively with relative humidity (r = −0.75), water vapour (r = −0.64), and precipitation (r = −0.51), confirming efficient wet removal of aerosols, while the near-zero wind relationship (r = −0.04) implies local combustion control.

The Coastal zone (Abidjan, Ivory Coast) exhibits comparable negative correlations with moisture (r = −0.40 to −0.57) and wind speed (r = −0.44), suggesting that rainfall and marine humidity inhibit the accumulation of aerosols. Coastal locations in Cameroon (Douala, Limbe, and Buea) similarly exhibit patterns consistent with those reported for southern West Africa, where negative associations with precipitation and humidity are indicative of the role of wet scavenging in reducing aerosol accumulation. However, the continuous occurrence of moderate AOD levels suggests that persistent contributions are coming from urban activity and coastal sources.

Comparative Insights and Likely Causes

A clear north-south gradient emerges. In the Sahara and Sahel, dust uplift is associated with strong temperature and wind correlations alongside lower levels of precipitation. The Sudanian zone shows the greatest climatic sensitivity, as combined biomass burning and dust transport yield the highest coefficients (temperature r = 0.74; precipitation r = −0.67). By contrast, the Guinean and Coastal zones display weaker overall correlations due to rainfall and humidity buffering aerosol effects, though combustion aerosols remain significant, especially through wind dispersion. Overall, the spatial variability reflects the balance of dominant sources – dust in the arid north, biomass burning in the transitional belt, and combustion or industrial emissions in the humid south – modulated by each zone's climatological background.

The structure of aerosol loading and climatic interactions across West Africa was illustrated by the scatter matrix plots in Fig. 3a-e. The plots reinforce the relationships observed in the correlation heatmaps in Fig. 2a-e. In the arid Sahara and Sahel zones, scatter patterns show positive slopes between AOD and temperature, indicating that elevated aerosol loading coincides with enhanced surface heating and dust uplift. There is wider scatter against wind speed, which further reflects aerosol entrainment by strong Harmattan winds typical of dry-season conditions. In the Sudanian and Guinean zones, the strong clustering between AOD and $PM_{2.5}$ confirms that fine particulates – largely from biomass burning and mixed dust from anthropogenic sources dominate regional optical depth. The southern Coastal zone exhibits steep negative slopes with precipitation, humidity, and water vapour, showing the efficiency of wet scavenging and dilution processes in humid marine environments.

Aerosol hotspots are therefore more pronounced under hot, dry, and windy conditions but weaken under humid, convective regimes. This suggests a north-south gradient in aerosol-climate relationships, with dust-driven loading in the north transitioning to combustion- and urban-dominated emissions in the south.

4.2. Seasonal variability of aerosol optical depth and regional contributions (%RAOD)

Seasonal cycles of aerosol loading (Fig. 4; Table 4) display pronounced north–south contrasts across West African climate zones and part of Central Africa, reflecting the timing of dust outbreaks, biomass burning, and urban-industrial emissions. In the Sahara zone, peaks occurred in summer months, with Araouane (Mali) reaching 0.74 in June and Taoudenni (Mali) reaching 0.62 in July. These maxima correspond to the boreal summer (June–August), when strong surface winds and dry soils favour large–scale dust uplift and transport. This pattern is consistent with long–term observations of the Saharan dust season, when convective activity and the Saharan Heat Low drive enhanced emissions and long–range transport.

The Sahelian zone displayed earlier peaks in late dry–season months. Fada N'gourma (Burkina Faso) recorded 0.80 in March, while in the extension into Chad, Abeche and Moussoro recorded 0.66 and 0.76 in April, respectively. These maxima reflect the combined

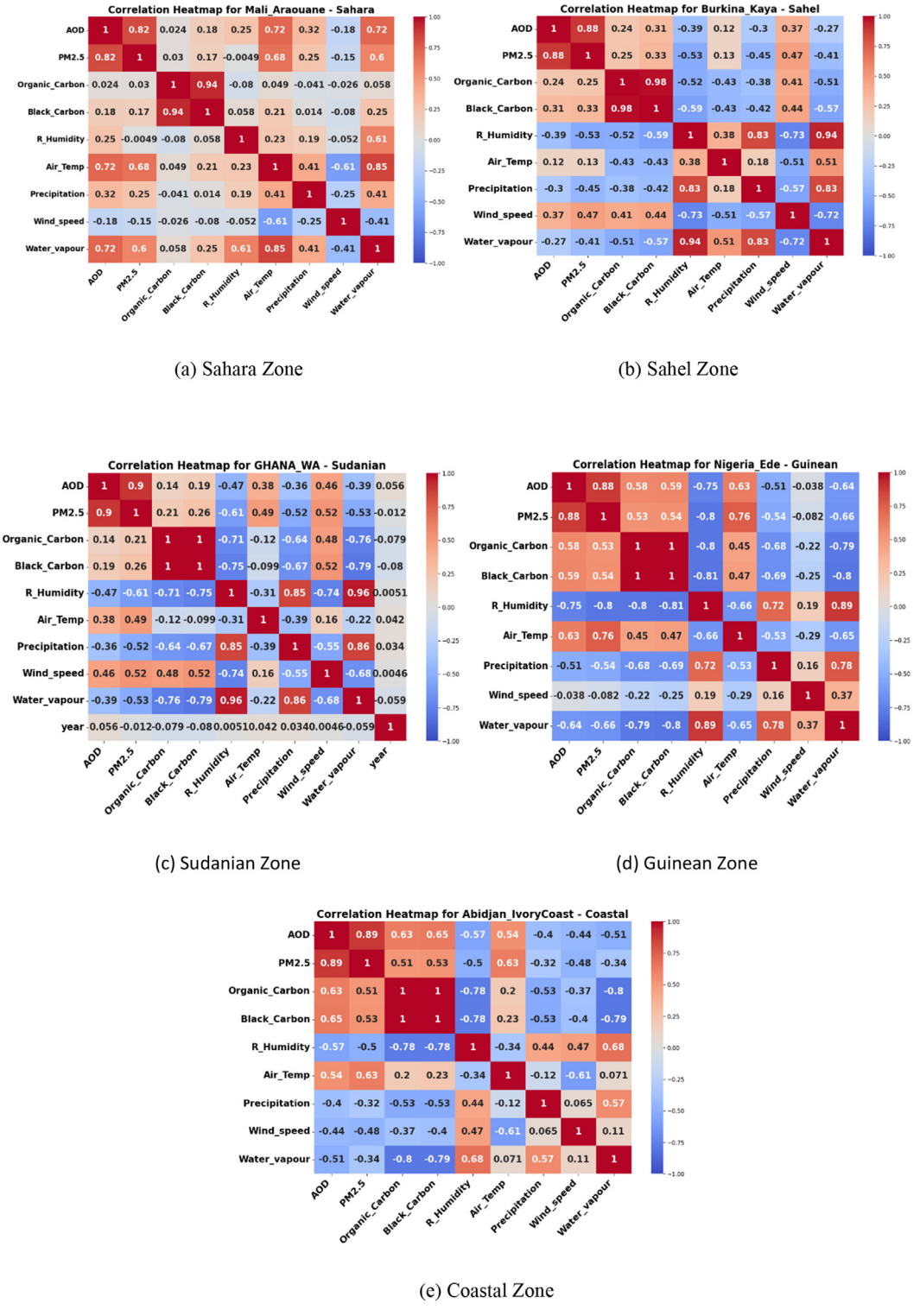

Fig. 2. (a–e) Correlation heatmaps showing relationships between aerosol loading (AOD, BC, OC, $PM_{2.5}$) and climatic parameters (temperature, precipitation, humidity, wind speed) across the five West African climate zones. Positive correlations dominate with temperature and wind speed in the arid north (Sahara, Sahel), while negative associations with precipitation and humidity are strongest in the Sudanian zone. The Guinean and Coastal zones reflect combustion and urban-industrial influences moderated by rainfall.

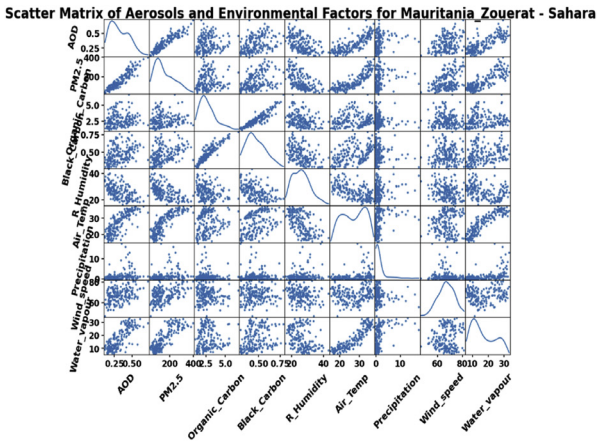

(a) Sahara Zone

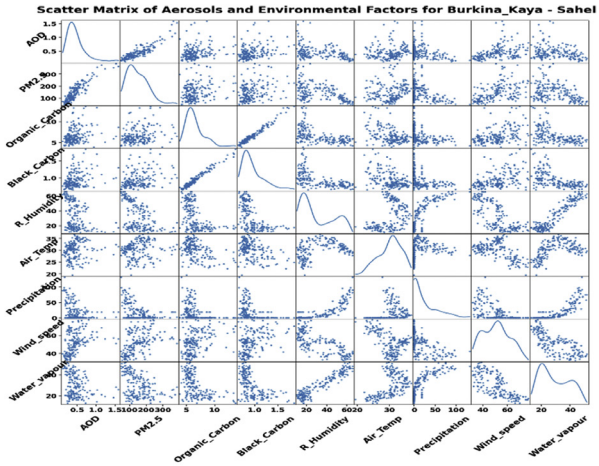

(b) Sahel Zone

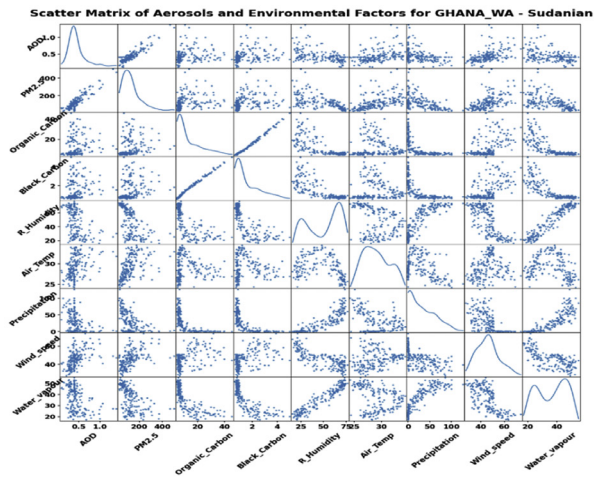

(c) Sudanian Zone

Fig. 3. (a–e) Scatter plots showing relationships between aerosol variables (AOD, BC, OC, $PM_{2.5}$) and climatic parameters (temperature, precipitation, relative humidity, wind speed) across the five West African climate zones. Positive links with temperature and wind speed and negative links with precipitation and humidity confirm that aerosols consistently warm the atmosphere and suppress rainfall, with varying intensity across zones.

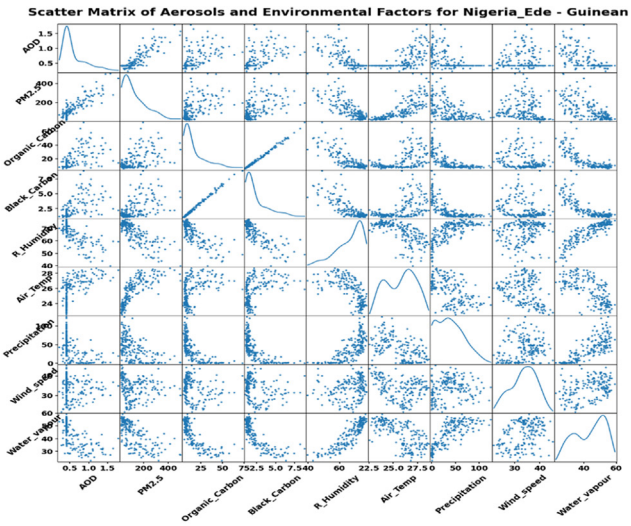

(d) Guinean Zone

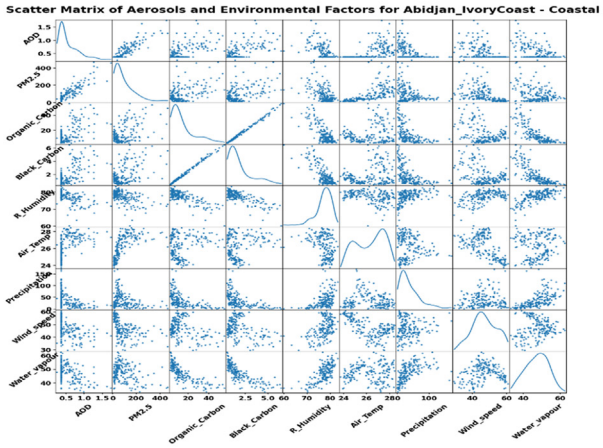

(e) Coastal Zone

Fig. 3. Continued

effects of dust advection and biomass burning during February to April, characteristic of the Harmattan period. Ogunjo [28] similarly observed that dust and biomass burning dominate aerosol loading across the Sahel and tropical Nigeria during this period.

In the Sudanian zone, February maxima dominated, with Kano (Nigeria) recording 1.07, Kaduna 0.92, and Jos 0.78. These peaks highlight the contribution of widespread savanna biomass burning, compounded by transported dust intrusions from the Sahel. Ochei et al. [8] confirmed that carbonaceous aerosols from fire activity are abundant in this zone during the dry season, showing strong negative relationships with rainfall and positive associations with regional temperature. The Guinean and Coastal zones recorded the highest overall AOD values, shaped largely by combustion and urban-industrial sources. Lagos peaked at 1.35 in February, while Ede and Warri both recorded 1.18. These maxima occurred in the heart of the dry season (Jan-Feb), when stagnant conditions favour the accumulation of pollution from biomass burning and the use of fossil fuels. Even during the wet season, Lagos maintained relatively elevated values, reflecting its urban-industrial intensity. A recent work by Akinyoola et al., [25] supported the fact that absorbing aerosols, particularly black carbon, are associated with enhanced regional warming and extreme events in southern West Africa, and is consistent with these findings. The Coastal locations in Cameroon (Douala, Limbe, and Buea) display consistent AOD values of ~0.87 in February, showing moderate aerosol presence. Unlike major West African urban centres such as Lagos, aerosol levels in these locations are lower, but constant due to a balance between emission sources and efficient wet removal mechanisms associated with high humidity and rainfall.

The %RAOD contributions presented in Table 2 further emphasized the dominance of individual hotspots. Araouane accounted for 17.11% of Sahara AOD in 2018, Fada N'gourma 14.47% of Sahel AOD in 2016, Kano 16.48% of Sudanian AOD in 2020, and

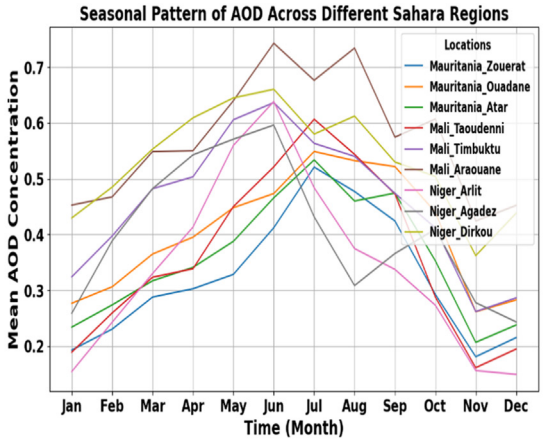

(i) Sahara Zone

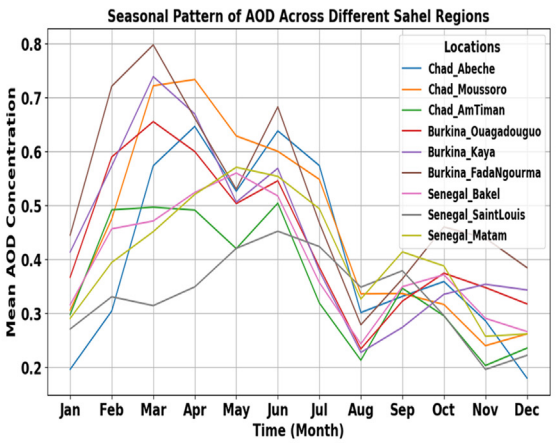

(ii) Sahel zone

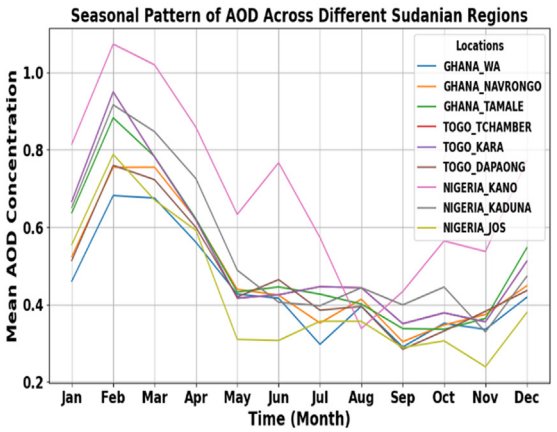

(iii) Sudanian zone

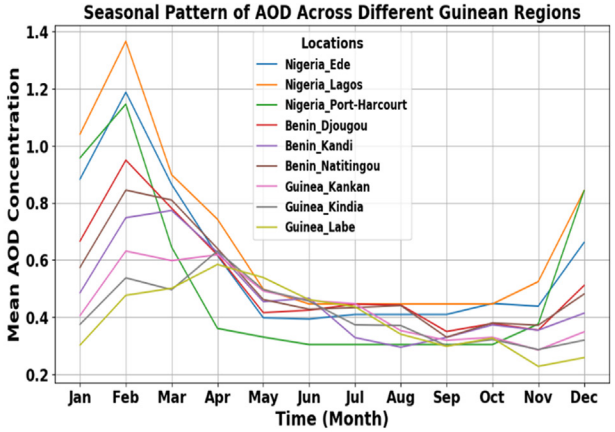

(iv) Guinean Zone

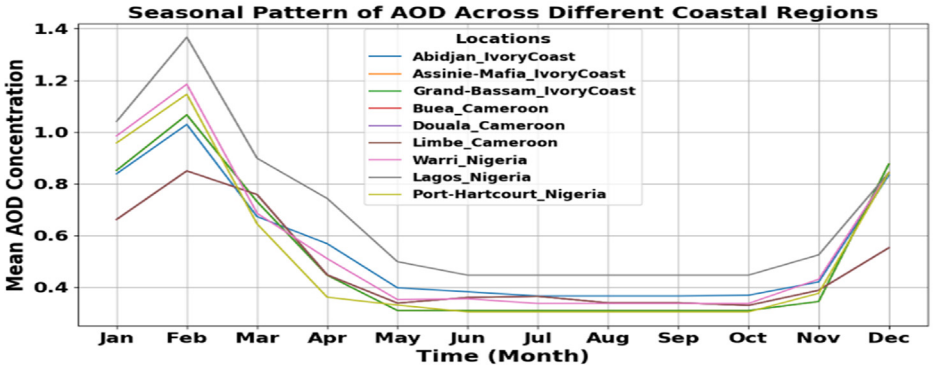

(v) Coastal Zone

Fig. 4. (i–v) Seasonal variability of AOD across representative stations in the five West African climate zones (2008 – 2023). Peaks reflect dust uplift in the Sahara during summer and late dry season, biomass-burning dominance in the Sudanian in February, and combustion/urban-industrial contributions in the Guinean and Coastal zones during the winter dry season. The patterns reveal a clear north-south gradient in seasonal drivers of aerosol loading.

Table 2
Percentage relative AOD (%RAOD) contributions of representative stations within the five West African climate zones (Sahara, Sahel, Sudanian, Guinean, and Coastal) for the period 2008–2023. The table identifies dominant hotspots where individual locations, such as Araouane, Fada N'gourma, Kano, and Lagos, contributed disproportionately to zonal aerosol burdens.

Time (Year)	Mauritania (%RAOD)			Mali (%RAOD)			Niger (%RAOD)		
	Zouerat	Ouadane	Atar	Taoudenni	Timbuktu	Araouane	Arlit	Agadez	Dirkou
2008	8.99	11.11	10.05	9.52	12.43	**14.81**	**8.73**	11.11	13.49
2009	**7.92**	10.66	9.29	8.47	12.84	**15.03**	9.56	11.75	14.75
2010	**8.17**	10.89	9.16	9.65	12.62	**14.60**	10.40	11.14	13.61
2011	**7.87**	10.24	8.66	9.97	12.34	**15.49**	9.97	11.55	13.65
2012	**8.76**	11.08	9.02	9.54	12.37	**15.21**	**8.76**	10.57	13.92
2013	**8.33**	10.83	8.89	8.61	11.39	**16.11**	9.17	12.22	14.72
2014	**8.26**	10.19	**8.26**	9.92	12.95	**15.98**	10.19	10.47	14.05
2015	**8.18**	9.77	9.09	8.41	11.59	**13.18**	**8.18**	10.45	11.59
2016	**7.21**	9.30	8.14	8.14	11.40	**13.02**	9.53	11.16	13.49
2017	**8.56**	10.08	9.32	10.08	12.09	**14.86**	9.82	11.08	14.11
2018	**9.14**	11.50	10.91	10.91	13.57	**17.11**	10.32	10.91	16.22
2019	**8.24**	10.59	9.41	10.00	11.76	14.71	9.41	10.59	**15.59**
2020	9.19	11.42	10.86	9.75	11.42	**15.32**	**8.08**	9.75	13.93
2021	9.04	10.64	10.64	10.64	12.23	**15.69**	**7.98**	9.57	13.83
2022	9.39	11.68	10.66	10.15	11.68	**15.74**	**7.11**	8.88	14.72
2023	8.70	11.59	9.28	9.57	11.01	**16.23**	**8.41**	10.43	15.07

(a)

Time (Year)	Chad (%RAOD)			Burkina Faso (%RAOD)			Senegal (%RAOD)		
	Abeche	Moussoro	Am-Timan	Ouagadougou	Kaya	Fada-N'gourma	Bakel	Saint Louis	Matam
2008	10.43	11.76	**9.09**	11.50	**12.83**	**12.83**	10.70	10.16	10.96
2009	12.63	12.63	11.02	11.02	**13.98**	12.10	8.87	**8.33**	9.14
2010	10.95	11.90	9.76	12.38	**13.57**	13.10	10.00	**8.33**	10.00
2011	11.38	**14.09**	10.30	10.84	12.20	12.74	10.84	**8.13**	9.21
2012	10.71	**12.76**	**9.44**	11.73	11.99	**12.76**	11.22	**9.44**	10.20
2013	11.84	**13.08**	10.28	11.84	11.21	12.46	9.66	**8.72**	10.59
2014	10.73	11.58	9.60	11.30	10.45	**12.99**	11.86	**9.04**	12.15
2015	9.71	10.38	**8.80**	11.29	12.64	**15.12**	11.06	**8.80**	12.19
2016	11.42	11.68	10.66	11.17	12.18	**14.47**	9.39	**8.38**	10.41
2017	10.68	11.17	10.44	11.41	11.41	**13.59**	10.68	**9.47**	10.92
2018	10.88	10.88	9.59	11.40	10.10	**14.77**	11.40	**9.07**	12.18
2019	12.54	14.19	**9.57**	13.20	12.87	**16.50**	11.22	**9.57**	13.20
2020	11.88	15.51	**10.56**	15.84	14.19	**18.48**	13.53	**10.56**	15.18
2021	10.54	11.35	**8.92**	11.35	11.08	**13.51**	11.08	9.73	12.43
2022	10.08	12.85	8.56	12.34	12.09	**15.37**	9.57	**8.31**	10.33
2023	11.58	14.47	9.65	11.25	10.93	**14.79**	9.65	**8.36**	9.65

(b)

Time (Year)	Ghana (%RAOD)			Togo (%RAOD)			Nigeria (%RAOD)		
	Wa	Navrongo	Tamale	Tchamber	Kara	Dapaong	Kano	Kaduna	Jos
2008	**8.76**	10.39	11.00	11.00	11.00	9.37	**16.29**	13.03	9.57
2009	**9.51**	9.74	10.21	11.37	11.37	9.74	**15.55**	12.06	10.44
2010	10.22	11.09	10.65	10.87	10.87	10.65	**14.57**	11.96	**8.91**
2011	10.14	9.91	10.85	11.79	11.79	9.67	**14.62**	12.03	**9.43**
2012	9.65	11.09	11.50	11.50	11.50	10.27	**13.96**	11.29	**9.45**
2013	**8.85**	10.16	11.20	11.72	11.72	10.42	**14.06**	11.98	9.90
2014	**9.20**	9.95	11.94	11.94	11.94	10.45	**14.18**	11.44	9.45
2015	9.42	10.14	11.59	11.41	11.41	9.96	**15.58**	11.96	**8.51**
2016	9.20	10.00	11.20	11.00	11.00	10.40	**16.00**	12.00	**9.00**
2017	**9.35**	9.55	11.38	11.38	11.38	10.37	**14.84**	11.79	9.96
2018	9.89	10.53	11.16	11.37	11.37	10.53	**15.58**	11.16	**8.42**
2019	10.08	11.34	11.84	11.08	11.08	10.33	**13.85**	11.34	**9.07**
2020	10.38	10.84	10.84	11.96	11.96	11.51	**16.48**	11.74	**9.03**
2021	9.18	10.41	11.84	11.63	11.63	10.61	**14.69**	11.22	**8.57**
2022	9.63	10.61	10.61	11.39	11.39	10.22	**15.72**	11.20	**9.23**
2023	**9.21**	10.06	11.56	11.78	11.78	9.64	**14.56**	11.99	9.64

(continued on next page)

Table 2
(*continued*)

(c)

Time (Year)	Nigeria (%RAOD)			Benin (%RAOD)			Guinea (%RAOD)		
	Ede	Lagos	P/H	Djougou	Kandi	Natitingou	Kankan	Kindia	Labe
2008	13.40	**14.47**	10.85	11.49	11.06	11.49	9.15	9.15	**8.94**
2009	12.85	**17.06**	9.81	11.45	10.51	10.98	9.58	9.35	**8.64**
2010	12.61	**13.03**	11.97	10.68	10.47	11.54	10.04	**9.62**	9.83
2011	**13.92**	13.68	**9.43**	11.79	10.14	10.61	11.08	9.91	9.91
2012	12.86	**16.12**	11.43	11.43	10.41	10.82	9.59	8.78	**8.57**
2013	13.35	**15.62**	12.09	11.34	**9.07**	10.58	10.08	9.57	**9.07**
2014	13.16	**14.32**	12.24	11.09	9.47	11.09	9.70	**9.24**	9.47
2015	13.10	**14.72**	8.47	12.70	11.69	11.90	10.08	8.87	**8.27**
2016	12.93	**14.66**	12.07	11.85	10.78	11.85	9.27	8.41	**7.97**
2017	13.88	**15.09**	12.07	11.27	10.06	11.07	9.26	8.65	**8.25**
2018	13.05	**13.50**	11.06	11.95	10.62	11.73	10.18	9.29	**8.85**
2019	12.59	**15.06**	11.60	10.86	10.37	11.85	9.88	9.14	**8.64**
2020	12.61	**15.04**	12.17	11.73	10.62	11.50	9.07	**8.63**	**8.63**
2021	13.52	**15.98**	12.70	11.68	9.43	11.07	9.43	8.40	**7.99**
2022	12.37	**14.88**	10.27	12.16	11.11	11.95	9.43	9.22	**8.39**
2023	12.08	**15.21**	12.75	12.30	9.62	11.41	9.17	9.40	**8.28**

(d)

Time (Year)	Ivory Coast (%RAOD)			Cameroon (%RAOD)			Nigeria (%RAOD)		
	Abidjan	Assinie-Mafia	Grand-Bassam	Buea	Douala	Limbe	Warri	Lagos	P/H
2008	13.92	11.56	11.56	**10.85**	**10.85**	**10.85**	12.97	**16.04**	12.03
2009	12.00	12.00	12.00	10.11	10.11	10.11	9.47	**15.37**	**8.84**
2010	11.25	11.45	11.45	**9.61**	**9.61**	**9.61**	13.29	**12.47**	**12.47**
2011	12.41	11.22	11.22	10.50	10.50	10.50	10.50	**13.84**	**9.55**
2012	10.71	11.47	11.47	**10.15**	**10.15**	**10.15**	**10.15**	**14.85**	10.53
2013	11.55	11.09	11.09	**9.93**	**9.93**	**9.93**	11.32	**14.32**	11.09
2014	11.66	11.66	11.66	**9.64**	**9.64**	**9.64**	10.09	**13.90**	11.88
2015	10.62	9.93	9.93	9.25	9.25	9.25	12.33	**12.50**	**7.19**
2016	11.45	11.45	11.45	**9.61**	**9.61**	**9.61**	11.25	**13.91**	11.45
2017	11.42	**9.82**	**9.82**	10.02	10.02	10.02	11.62	**15.03**	12.02
2018	11.09	10.08	10.08	11.29	11.29	11.29	**12.30**	**12.30**	10.08
2019	11.55	**10.16**	**10.16**	10.39	10.39	10.39	11.78	**14.09**	10.85
2020	11.46	**9.77**	**9.77**	10.40	10.40	10.40	11.25	**14.44**	11.68
2021	9.86	**8.96**	**8.96**	**8.96**	**8.96**	**8.96**	12.19	**13.98**	11.11
2022	11.06	10.21	10.21	**10.00**	**10.00**	**10.00**	13.19	**15.11**	10.43
2023	12.28	11.42	11.42	**8.84**	**8.84**	**8.84**	11.64	**16.66**	12.28

(e)

Lagos 17.06% of Guinean AOD in 2009. These results illustrate how single locations– whether dust-dominated (Araouane), biomass-burning influenced (Kano, Fada N'gourma), or urban-industrial (Lagos) – can outweigh the contributions of several rural stations combined.

Summarily, the seasonal variability results align with established climatology: dust dominates summer peaks in the Sahara and Sahel, biomass burning controls late dry-season maxima in the Sudanian belt, and combustion/urban-industrial activity drives dry-season peaks in the Guinean and Coastal zones. The %RAOD analysis highlights a few important hotspots (Araouane, Fada N'gourma, Kano, Lagos) that disproportionately shape regional aerosol burdens and their climatic effects, in agreement with recent observational and modeling studies across places in West Africa [8,25,28].

4.3. Interannual variability and the 2015 anomaly

Interannual analysis (Table 4) was derived by aggregating annual mean values of AOD and dividing by the number of locations for each zone (9) as listed in Table 3. This reinforces the spatial gradient observed across zones, with the Sudanian and Coastal regions recording the highest annual mean total AOD burdens. Importantly, 2015 emerged as an exceptional year in many zones, with annual mean totals peaking simultaneously across the regions: Sahara (0.4412), Sahel (0.4921), Sudanian (0.6134), Guinean (0.5510), and Coastal (0.5847). The coherence of these maxima across different climatic regimes may be associated with large-scale atmospheric forcing. Although circulation indices such as ENSO and NAO were not directly analyzed in this study, the observed synchrony across all zones suggests that more investigation is necessary to understand the role of large-scale climate drivers.

Table 3
Annual mean AOD values for each of the five West African climate zones [(a) Sahara, (b) Sahel, (c) Sudanian, (d) Guinean, and (e) Coastal] from 2008 to 2023. These values provide the baseline for assessing zonal differences in aerosol loading and serve as the input for aggregated totals presented in Table 4.

Year	Maurit Zouerat	Maurit Ouadane	Maurit Atar	Mali Taoudenni	Mali Timbuktu	Mali Araouane	Niger Artit	Niger Agadez	Niger Dirkou
2008	0.336333	0.423667	0.378833	0.355917	0.465583	0.555417	0.330500	0.419667	0.511000
2009	0.286833	0.385250	0.335917	0.314250	0.474667	0.553250	0.346167	0.432000	0.535833
2010	0.334917	0.436583	0.374833	0.385000	0.505083	0.586750	0.418083	0.447333	0.551833
2011	0.301750	0.392417	0.325833	0.376333	0.472833	0.592583	0.378583	0.441750	0.523000
2012	0.344250	0.434667	0.354250	0.369417	0.481333	0.592583	0.342417	0.414583	0.543917
2013	0.399417	0.387167	0.315167	0.314167	0.414917	0.578167	0.325417	0.437333	0.530083
2014	0.302083	0.369833	0.298417	0.359000	0.466500	0.577083	0.365667	0.381667	0.509500
2015	0.356833	0.432333	0.400583	0.372250	0.505750	0.579667	0.356167	0.456417	0.510750
2016	0.311333	0.398667	0.352250	0.347667	0.487250	0.558167	0.408167	0.479583	0.575500
2017	0.343250	0.397250	0.372667	0.397417	0.480833	0.589583	0.388917	0.438833	0.557333
2018	0.313750	0.393667	0.368667	0.372833	0.461583	0.578750	0.347583	0.374333	0.553750
2019	0.279583	0.356082	0.318083	0.341833	0.396333	0.503333	0.317333	0.360250	0.526000
2020	0.331917	0.410000	0.389250	0.352333	0.406583	0.553500	0.293250	0.352417	0.501000
2021	0.335167	0.401167	0.398417	0.404833	0.456167	0.587583	0.296417	0.359833	0.520417
2022	0.374500	0.455167	0.415083	0.401917	0.461250	0.618750	0.283500	0.349500	0.576417
2023	0.302000	0.396833	0.316000	0.333917	0.379917	0.556500	0.286833	0.357250	0.519750

(a)

Year	Chad Abeche	Chad Moussoro	Chad AmTiman	Burkina Ouagadougou	Burkina Kaya	Burkina F.Ngourma	Senegal Bakel	Senegal St,Louis	Senegal Matam
2008	0.388000	0.437583	0.340750	0.430250	0.476833	0.477833	0.399750	0.384250	0.407833
2009	0.472417	0.471083	0.406417	0.411167	0.521500	0.454500	0.334333	0.313333	0.339667
2010	0.458833	0.495333	0.412917	0.523250	0.572583	0.546833	0.423333	0.351833	0.416000
2011	0.421833	0.519083	0.375750	0.403917	0.454083	0.470227	0.403000	0.301917	0.335667
2012	0.420500	0.495833	0.368500	0.463083	0.468333	0.497750	0.437333	0.371500	0.398250
2013	0.379667	0.423667	0.333833	0.379947	0.364417	0.402583	0.307167	0.281250	0.335333
2014	0.383833	0.413250	0.337167	0.395030	0.374167	0.464083	0.416917	0.321583	0.433667
2015	0.430583	0.458500	0.390083	0.504750	0.563750	0.666167	0.486750	0.386167	0.542000
2016	0.452833	0.463250	0.415083	0.436167	0.479333	0.574250	0.372333	0.332167	0.413833
2017	0.441917	0.464083	0.433667	0.473083	0.472417	0.555417	0.444417	0.390000	0.448417
2018	0.423500	0.422917	0.366750	0.438363	0.388833	0.568144	0.439750	0.349500	0.466583
2019	0.377000	0.427500	0.287667	0.396083	0.385833	0.501583	0.335083	0.290250	0.404417
2020	0.358247	0.471140	0.319753	0.476863	0.426417	0.561894	0.413161	0.323833	0.460761
2021	0.387750	0.423167	0.327000	0.423583	0.412917	0.500333	0.409917	0.356333	0.458167
2022	0.404833	0.510167	0.339917	0.492667	0.482000	0.611000	0.384750	0.332917	0.410667
2023	0.359667	0.448417	0.303250	0.348333	0.339000	0.463000	0.295583	0.255667	0.297667

(b)

Year	Ghana WA	Ghana Navrongo	Ghana Tamale	Togo Tchamber	Togo Kara	Togo Dapaong	Nigeria Kano	Nigeria Kaduna	Nigeria Jos
2008	0.425446	0.506780	0.536084	0.539742	0.539742	0.462142	0.795000	0.636947	0.470050
2009	0.413362	0.417182	0.442168	0.488909	0.488909	0.418475	0.674333	0.519864	0.447633
2010	0.474279	0.508932	0.488251	0.503492	0.503492	0.492975	0.667833	0.550061	0.406633
2011	0.425612	0.419849	0.464876	0.496576	0.496576	0.409809	0.615583	0.510644	0.402741
2012	0.474029	0.536614	0.559210	0.555826	0.555826	0.497617	0.676500	0.552811	0.458491
2013	0.343029	0.393864	0.425710	0.449405	0.449405	0.400951	0.541667	0.455530	0.377299
2014	0.367279	0.397015	0.475001	0.477992	0.477992	0.416534	0.566750	0.457614	0.382466
2015	0.515612	0.556932	0.644543	0.629909	0.629909	0.554975	0.863667	0.659144	0.465633
2016	0.460583	0.501417	0.561960	0.552992	0.552992	0.515617	0.803917	0.595644	0.453824
2017	0.464917	0.473417	0.561210	0.556409	0.556409	0.511367	0.733000	0.576530	0.490800
2018	0.474696	0.499864	0.528834	0.536492	0.536492	0.495392	0.743833	0.530697	0.406049
2019	0.399225	0.450447	0.466752	0.440322	0.440322	0.410784	0.552667	0.445644	0.364049
2020	0.457392	0.479099	0.479375	0.527822	0.527822	0.510534	0.729529	0.523008	0.396824
2021	0.454308	0.514780	0.575251	0.570576	0.570576	0.521034	0.724833	0.548644	0.418824
2022	0.492892	0.540879	0.536376	0.581238	0.581238	0.520842	0.802779	0.569311	0.468633
2023	0.431975	0.474212	0.535710	0.545322	0.545322	0.447534	0.684833	0.558197	0.448766

(continued on next page)

Table 3
(*continued*)

(c)

Year	Nigeria Ede	Nigeria Lagos	Nigeria PH	Benin Djougou	Benin Kandi	Benin Natitingou	Guinea Kankan	Guinea Kindia	Guinea Labe
2008	0.630800	0.682281	0.514548	0.539742	0.516197	0.538550	0.428917	0.426833	0.419282
2009	0.545792	0.733165	0.417965	0.488909	0.449667	0.473333	0.408986	0.400433	0.366750
2010	0.591034	0.613748	0.556691	0.503492	0.494917	0.539300	0.465083	0.447950	0.464480
2011	0.591117	0.575597	0.397489	0.496576	0.425167	0.453484	0.469069	0.415017	0.418750
2012	0.627617	0.786398	0.560191	0.555826	0.507114	0.531634	0.473971	0.434200	0.421897
2013	0.525442	0.616898	0.480382	0.449405	0.362000	0.417967	0.397471	0.384549	0.356115
2014	0.571951	0.620814	0.529382	0.477992	0.406833	0.478884	0.424569	0.402500	0.413782
2015	0.652875	0.732481	0.421239	0.629909	0.579890	0.593300	0.501374	0.437517	0.410583
2016	0.596209	0.681948	0.562774	0.552992	0.498417	0.545800	0.434500	0.394450	0.368198
2017	0.694384	0.753832	0.597084	0.556409	0.502724	0.552467	0.462471	0.434933	0.414532
2018	0.594776	0.606097	0.503798	0.536492	0.477640	0.527300	0.455805	0.418767	0.396615
2019	0.508709	0.613615	0.473132	0.440322	0.419667	0.475900	0.397250	0.370350	0.347333
2020	0.573634	0.681415	0.549750	0.527822	0.482474	0.517300	0.406236	0.391450	0.386948
2021	0.659542	0.779198	0.615500	0.570576	0.458500	0.540150	0.460486	0.405517	0.385833
2022	0.594125	0.707531	0.491417	0.581238	0.527614	0.572784	0.453652	0.436216	0.402980
2023	0.538034	0.677281	0.569750	0.545322	0.427167	0.506550	0.410917	0.423583	0.366948

(d)

Year	Ivory Abidjan	Ivory A.Mafia	Ivory G.Bassam	Cameroon Buea	Cameroon Douala	Cameroon Limbe	Nigeria Warri	Nigeria Lagos	Nigeria PH
2008	0.586610	0.494576	0.494576	0.456119	0.456119	0.456119	0.550509	0.682281	0.514548
2009	0.565527	0.565495	0.565495	0.484952	0.484952	0.484952	0.447796	0.733165	0.417965
2010	0.548349	0.557604	0.557604	0.467699	0.467699	0.467699	0.654823	0.613748	0.556691
2011	0.524921	0.469742	0.469742	0.440035	0.440035	0.440035	0.436629	0.575597	0.397489
2012	0.572027	0.614966	0.614966	0.543995	0.543995	0.543995	0.544059	0.786398	0.560191
2013	0.496110	0.477604	0.477604	0.428826	0.428826	0.428826	0.494212	0.616898	0.480382
2014	0.518421	0.516716	0.516716	0.434742	0.434742	0.434742	0.449865	0.620814	0.529382
2015	0.623588	0.576354	0.576354	0.538495	0.538495	0.538495	0.716836	0.732481	0.421239
2016	0.563754	0.558271	0.558271	0.470826	0.470826	0.470826	0.552892	0.681948	0.562774
2017	0.570932	0.488659	0.488659	0.502411	0.502411	0.502411	0.578976	0.753832	0.597084
2018	0.553671	0.503383	0.503383	0.556704	0.556704	0.556704	0.613656	0.606097	0.503798
2019	0.499004	0.441078	0.441078	0.451619	0.451619	0.451619	0.507559	0.613615	0.473132
2020	0.543182	0.461909	0.461909	0.492661	0.492661	0.492661	0.534976	0.681415	0.549750
2021	0.552038	0.498326	0.498326	0.496454	0.496454	0.496454	0.676073	0.779198	0.615500
2022	0.519838	0.481104	0.481104	0.466326	0.466326	0.466326	0.623419	0.707531	0.491417
2023	0.573266	0.525909	0.525909	0.406535	0.406535	0.406535	0.543642	0.677281	0.569750

(e)

Table 4
Zonal Annual Mean of AOD for the climate zones in West Africa and part of Central Africa, derived from the mean values in Table 3. The zonal annual mean highlights interannual variability and reveals exceptional years such as 2015, when simultaneous maxima were recorded across the zones.

Time (Year)	Sahara Zone	Sahel Zone	Sudanian Zone	Guinean Zone	Coastal Zone
2008	0.4197	0.4159	0.5458	0.5219	0.5213
2009	0.4071	0.4138	0.4790	0.4761	0.5278
2010	0.4489	0.4668	0.5107	0.5196	0.5435
2011	0.4228	0.4095	0.4714	0.4714	0.4660
2012	0.4308	0.4357	0.5408	0.5443	0.4916
2013	0.4003	0.3564	0.4263	0.4434	0.4876
2014	0.4033	0.3993	0.4465	0.4807	0.4951
2015	0.4412	0.4921	0.6134	0.5510	0.5847
2016	0.4354	0.4377	0.5554	0.5150	0.5434
2017	0.4407	0.4582	0.5471	0.5501	0.5539
2018	0.4183	0.4294	0.5280	0.5019	0.5505
2019	0.3776	0.3784	0.4411	0.4496	0.4811
2020	0.3989	0.4236	0.5146	0.5019	0.5235
2021	0.4178	0.4110	0.5443	0.5417	0.5676
2022	0.4373	0.4410	0.5660	0.5297	0.5226
2023	0.3832	0.3456	0.5191	0.4962	0.5150

4.4. Trends of aerosol concentration over time

Fig. 5 and Table 4 illustrate interannual variability of aerosol optical depth (AOD) and associated aerosol concentrations across the five West African climate zones and selected representative locations from 2008 to 2023. The results highlight both a clear north-south gradient and marked temporal anomalies, underscoring the climatic sensitivity of aerosol loading in the region.

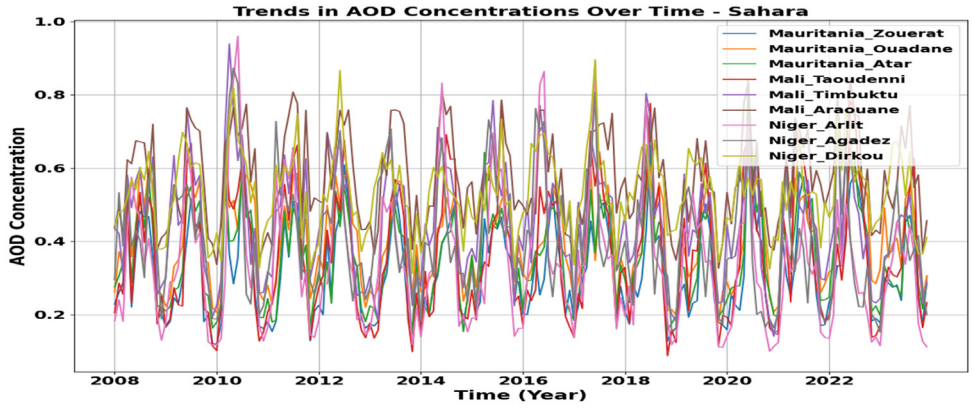

a (i)

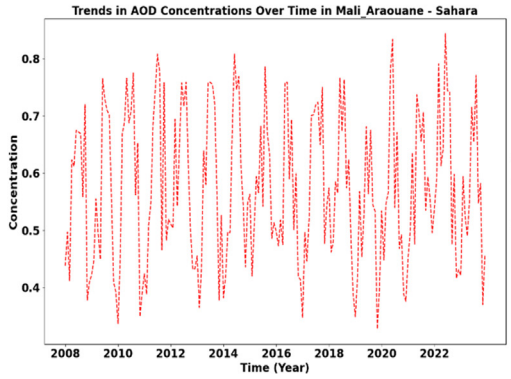

a (ii)

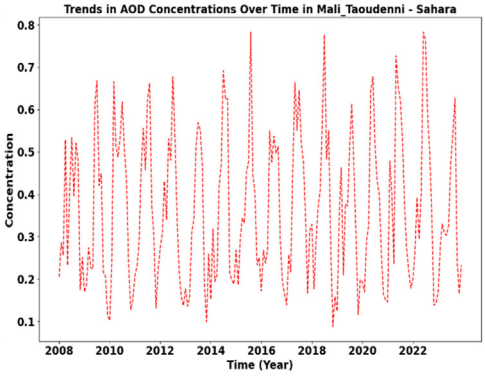

a (iii)

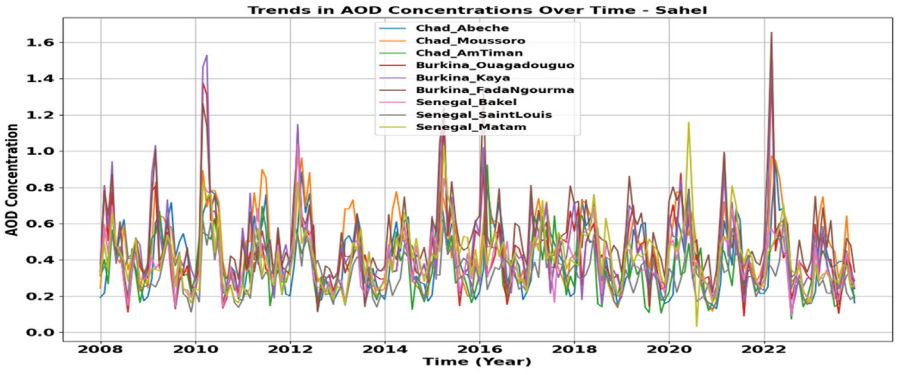

b (i)

Fig. 5. Representative plots showing the trends in AOD concentration across the five WA climate zones (2008–2023). Panels a(i)-d(i) illustrate zonal trends in AOD over time for the Sahara, Sahel, Sudanian, Guinean, and Coastal zones, respectively; panels a (ii-iii), b (ii-iii), c (ii-iv), and d (iii-v) compare AOD variations among representative locations across zones. The plots highlight interannual variability, zonal differences, and distinct aerosol loading patterns associated with dust uplift, biomass, and urban-industrial emissions across WA.

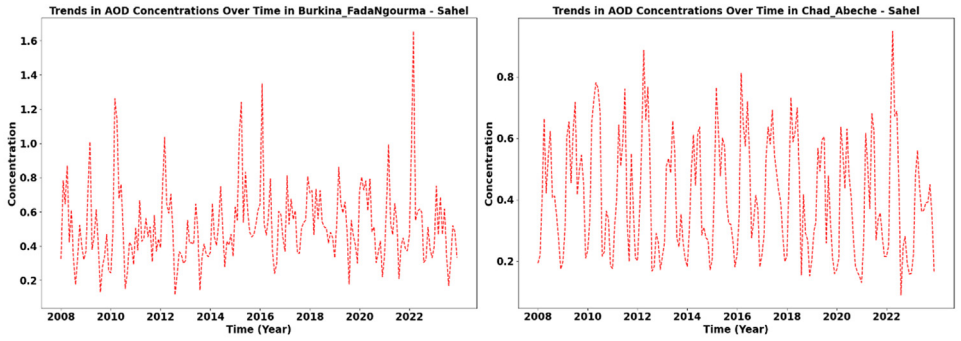

b (ii) b (iii)

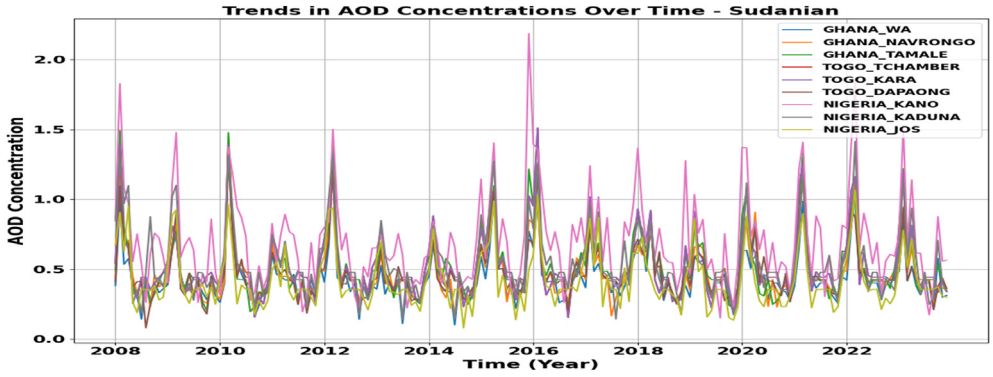

c (i)

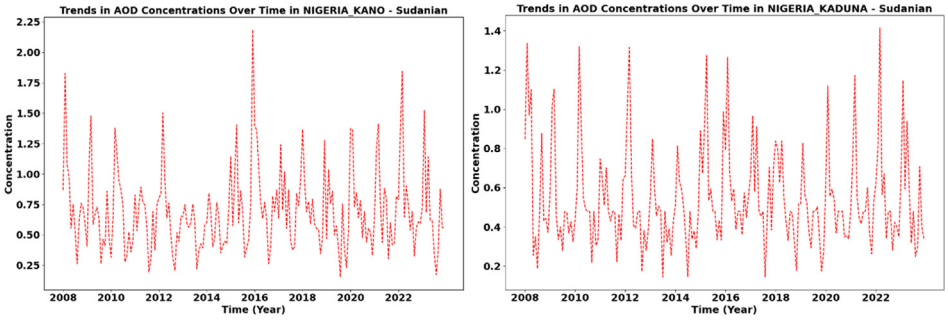

c (ii) c (iii)

Fig. 5. Continued

In the Sahara zone, long-term trends reflect episodic but high-magnitude dust events, with Araouane and Taoudenni showing recurrent summer peaks. Although variability is large, years of intensified dust mobilization (e.g., 2015 and 2020) stand out, with Araouane contributing up to 17.11% of zonal AOD in 2018. The Sahel displayed a similar but weaker (slightly) trajectory, with Fada N'gourma (18.48% in 2020, the highest across all zones) and Abeche showing strong late dry season contributions. These results confirm that dust advection combined with biomass burning dominates northern AOD variability.

The Sudanian zone exhibited the highest sensitivity, with Kano, Kaduna, and Jos consistently peaking during February and March. Kano alone contributed 16.48% of zonal AOD in 2020, underlining the dominance of localized biomass burning combined with transported dust. The trend indicates that even in wetter years, background AOD remains elevated, reflecting the persistence of anthropogenic activity. The Guinean and Coastal zones recorded the largest absolute AOD values. Lagos peaked at 1.35 in February 2009, contributing 17.06% of zonal AOD that year, while Port Harcourt and Warri showed sustained elevated burdens. Unlike the north, where wet deposition rapidly suppresses aerosols during the rainy season, these urban-industrial hotspots maintain high

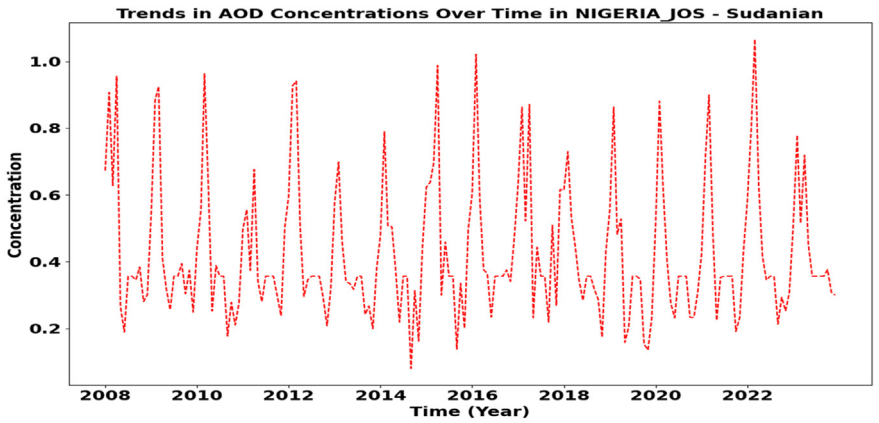

c (iv)

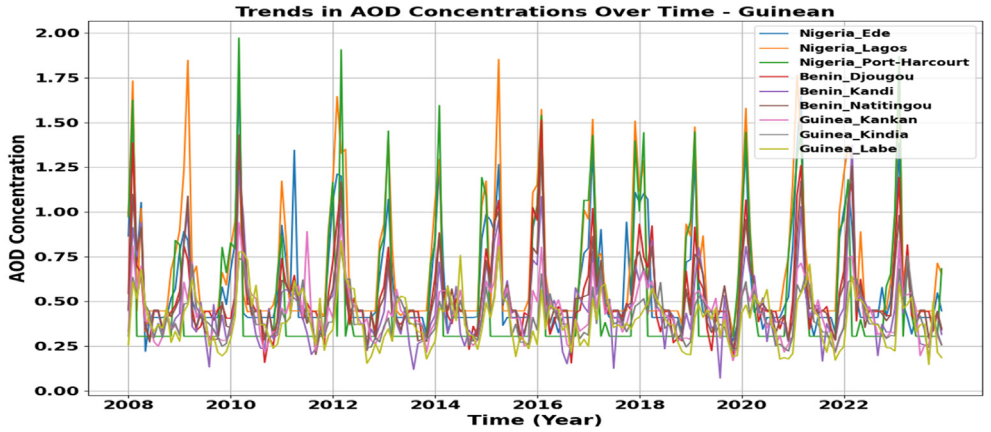

d (i)

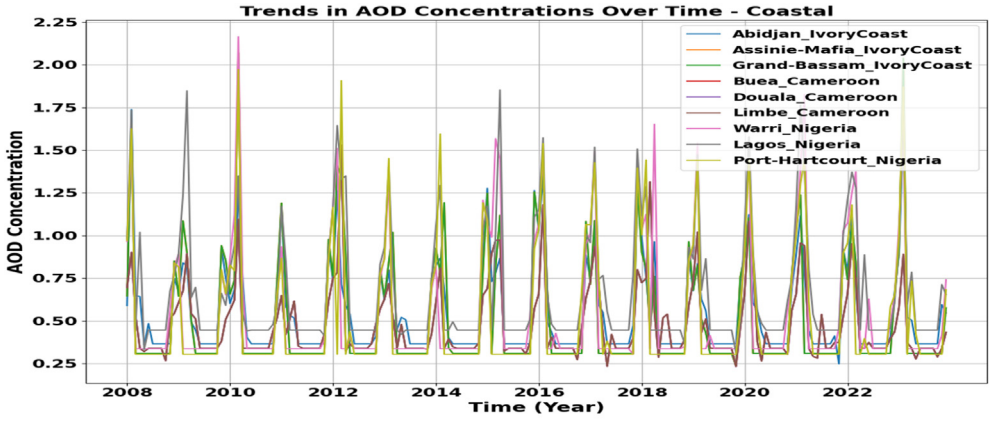

d(ii)

Fig. 5. Continued

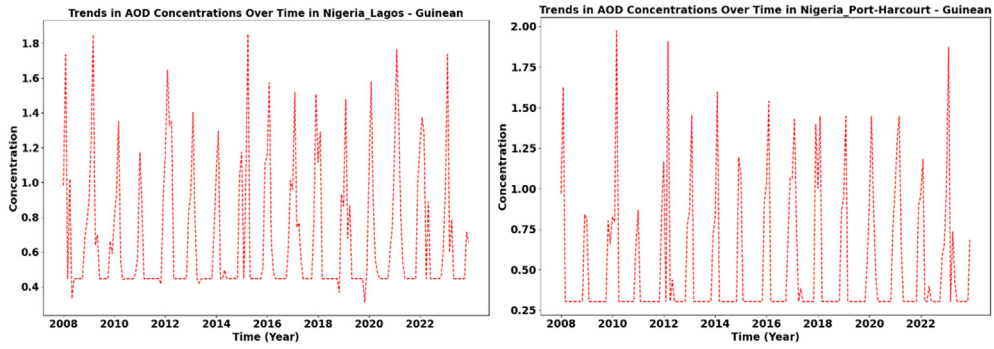

d (iii) d (iv)

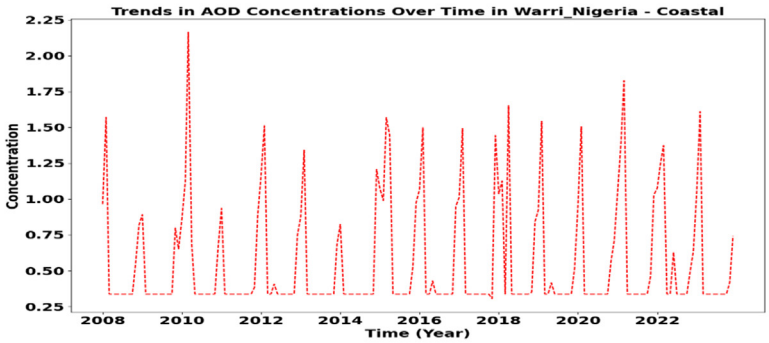

d (v)

Fig. 5. Continued

concentrations year-round due to continuous combustion and industrial emissions. The persistence of elevated AOD despite rainfall may indicate the increasing influence of anthropogenic emissions in southern West Africa.

Interannual variability revealed 2015 as a region-wide anomaly with simultaneous zonal mean AOD maxima across all zones (Sahara 0.4412; Sahel 0.4921; Sudanian 0.6134; Guinean 0.5510; Coastal 0.5847). This synchrony suggests a large-scale driver, likely ENSO-related drought, and the West African. Monsoon weakening, which intensified dust mobilization, biomass burning, and reduced wet deposition. The anomaly highlights the capacity of regional and global climate modes to amplify aerosol loading across contrasting environments. In Chad, interannual variability reflects Sahelian dynamics in Abeche and Moussoro, showing consistent contributions to zonal AOD up to ~15.51% in 2020, suggesting the effect of transported and local aerosols. In contrast, Buea, Douala, and Limbe in Cameroon have shown relatively stable, though moderate, contributions to AOD (~8.84 to 11.29%), suggesting less variability but persistent aerosol presence attributed to urban activities and atmospheric moisture conditions.

Summarily, Fig. 5 demonstrates that while dust dominates episodic peaks in the arid north, biomass burning and urban-industrial emissions sustain long-term increases in the Sudanian and southern zones. The AOD trends confirm that localized hotspots such as Fada N'gourma, Kano, and Lagos exert disproportionate influence on zonal burdens. These findings emphasize the importance of incorporating both natural and man-made trends into climate models to capture aerosol-climate interactions in West Africa.

5. Conclusion

This study analyzed 16 years (2008–2023) of satellite data to examine aerosol concentration variations and their climatic associations across five West African zones. Results demonstrated consistent aerosol–climate association: positive correlations with temperature and wind speed, and negative associations with precipitation and humidity. The Sudanian (AOD–temperature $r = 0.74$; AOD–precipitation $r = -0.67$), and Sahara zones ($r = 0.72$; -0.63) exhibited the strongest sensitivities, reflecting the combined influence of biomass burning, dust intrusions, and synoptic-scale circulation.

Seasonal variability confirmed distinct zonal controls: dust uplift dominated summer peaks in the Sahara and Sahel; biomass burning drove February maxima in the Sudanian; and urban-industrial emissions sustained high burdens in the Guinean and Coastal zones, particularly at Lagos (1.35 in February) and Port Harcourt (>2.0). Importantly, the %RAOD analysis revealed the dominance of localized hotspots–Araouane contributed 17.11% of Sahara AOD in 2018, Fada N'gourma 18.48% of Sahel AOD in 2020, Kano 16.48% of Sudanian AOD in 2020, and Lagos 17.06% of Guinean AOD in 2009. These findings suggest that single urban or rural centers can outweigh multiple stations combined, making %RAOD a robust metric for identifying aerosol "hotspot contributors."

Interannual variability further highlighted 2015 as a regional anomaly, with simultaneous zonal mean AOD maxima across all zones: Sahara (0.4412), Sahel (0.4921), Sudanian (0.6134), Guinean (0.5510), and Coastal (0.5847). This synchrony may be linked to large-scale climate modes, including the probable influences of ENSO and West African Monsoon variability, which may enhance dust mobilization, biomass burning, and reduced wet deposition. However, the interpretations are inferred; no direct analysis of atmospheric circulation indices was conducted in this research work. It should therefore be considered as a plausible hypothesis requiring further validation in future studies. The inclusion of Chad and Cameroon shows that aerosol dynamics extend beyond typical West African boundaries. Chad reflects Sahelian dust-biomass interactions, while Cameroon exhibits aerosol behavior influenced by humidity, in alignment with the southern West African pattern.

Overall, a north–south gradient was evident: dust in the arid north, biomass in the transitional savanna, and industrial emissions in the humid south. By integrating %RAOD with seasonal and interannual patterns, this study provides a clearer framework for linking localized sources to regional climate impacts. These results underscore the urgency of incorporating hotspot dynamics into climate models and emission control strategies for West Africa.

6. Recommendation

This study demonstrates marked spatial and temporal contrasts in aerosol loading and its climatic impacts across West African zones. To strengthen regional resilience, a coordinated aerosol monitoring network which integrates ground and satellite observations (e.g., MODIS, MISR, MERRA-2, AIRS) is recommended, with emphasis on hotspot regions like Araouane, Fada N'gourma, Kano, Lagos, and Abidjan. Source-specific mitigation should target the stabilization of dust in arid zones, control of biomass burning in savannas, and stricter emission standards in coastal urban centres. Integrating AOD and %RAOD metrics into regional climate and air-quality models will enhance the prediction of monsoon variability and radiative forcing. Future studies should include atmospheric circulation indices such as ENSO and West African Monsoon metrics to investigate how large-scale climate drivers affect interannual aerosol variability across the regions. It is essential also to have a strengthened policy coordination and public-health awareness under ECOWAS and the AU, so as to mitigate aerosol-induced climate and air-quality risks.

Funding

"The authors declare that no funds, grants, or other support were received during the preparation of this manuscript."

Declaration of competing interest

The authors declare that they have no known competing financial interests or personal relationships that could have appeared to influence the work reported in this paper.

CRediT authorship contribution statement

Oluseye David Dare: Writing – original draft, Methodology, Formal analysis, Data curation. **Modupe E. Sanyaolu:** Writing – review & editing, Validation, Supervision, Methodology, Formal analysis, Conceptualization. **Ayodele O. Soge:** Writing – review & editing, Supervision, Resources, Investigation. **Alexander A. Willoughby:** Writing – review & editing, Supervision, Project administration.

Data availability

Data will be made available on request.

Acknowledgement

The National Aeronautics and Space Administration (NASA) are appreciated for their support to access the data used for this study.

References

[1] Abosede S. Alli, Sierra N. Clark, Jiayuan Wang, James Bennett, Allison F. Hughes, Majid Ezzati, Michael Brauer, James Nimo d, Josephine Bedford-Moses, Solomon Baah, Alicia Cavanaugh, Samuel Agyei-Mensah, George Owusu, Jill Baumgartner, Raphael E. Arku, High-resolution patterns and inequalities in ambient fine particle mass ($PM_{2.5}$) and black carbon (BC) in the Greater Accra Metropolis, Ghana, Sci. Total Environ. (2023), doi:10.1016/j.scitotenv.2023.162582.

[2] C. Tomasi, A. Lupi, Primary and secondary sources of atmospheric aerosol, in: C. Tomasi, S. Guzzi, A. Kokhanovsky (Eds.), Atmospheric Aerosols: Life Cycles and Effects on Air Quality and Climate, 1st edn., Wiley-VCH Verlag GmbH & Co. KGaA, 2017, pp. 1–86.

[3] K. Schepanski, I. Tegen, B. Laurent, B. Heinold, A. Macke, A new Saharan dust source activation frequency map derived from MSG-SEVIRI IR-channels, Geophys. Res. Lett. 34 (18) (2007), doi:10.1029/2007GL030168.

[4] F. De Longueville, P. Ozer, F. Gemenne, S. Henry, O. Mertz, J. Nielsen, Comparing climate change perceptions and meteorological data in rural West Africa to improve the understanding of household decisions to migrate, Clim. Change (2020), doi:10.1007/s10584-020-02704-7.

[5] Intergovernmental Panel on Climate ChangeThe Physical Sciences Basis. Contribution of Working Group I to the Fourth Assessment Report of the Intergovernmental Panel on Climate Change, S. Solomon, D. Qin, M. Manning, et al. (Eds.), Cambridge University Press, Cambridge, United Kingdom, 2007.

[6] A. Hollingsworth, R.J. Engelen, A. Benedetti, A. Dethof, J. Flemming, J.W. Kaiser, J.J. Morcrette, A.J. Simmons, C. Textor, O. Boucher, F. Chevallier, P. Rayner, H. Elbern, H. Eskes, C. Granier, V.H. Peuch, L. Rouil, M.G. Schultz, Toward a monitoring and forecasting system for atmospheric composition: the gems project, B. Am. Meteorol. Soc. 89 (2008) 1147–1164, doi:10.1175/2008BAMS2355.1.
[7] J.L. Zhang, J.S. Reid, D.L. Westphal, N. Baker, E.J. Hyer, A system for operational aerosol optical depth data assimilation over global oceans, J. Geophys. Res. 113 (2008) D10208, doi:10.1029/2007JD009065.
[8] M. Ochei, A. Oluleye, R. Wolke, D. Pratt, T. Njie, Aerosols' variability and their relationship with climatic parameters over West Africa, Environ. Monit. Assess. (2023), doi:10.1007/s10661-023-11204-x.
[9] J. Haywood, P. Francis, M. Glew, J. Taylor, Optical properties and direct radiative effect of Saharan dust: a case study of two Saharan dust outbreaks using aircraft data, J. Geophys. Res. 106 (2001) 18417–18430.
[10] Intergovernmental Panel on Climate Change, in: The Physical Science Basis, Cambridge University Press, 2013, p. 1535, doi:10.1017/CBO9781107415324.
[11] A.J. Adesina, K.R. Kumar, V. Sivakumar, Aerosol-cloud-precipitation interactions over major cities in South Africa: impact on regional environment and climate change, AAQR (2016), doi:10.4209/aaqr.2015.03.0185.
[12] U. Lohmann, L. Rotstayn, T. Storelvmo, A. Jones, S. Menon, J. Quaas, A.M.L. Ekman, D. Koch, R. Ruedy, Total aerosol effect: radiative forcing or radiative flux perturbation? Atmos. Chem. Phys. (2010), doi:10.5194/acp-10-3235-2010.
[13] B. Mai, X. Deng, Z. Li, et al., Aerosol optical properties and radiative impacts in the Pearl River Delta region of China during the dry season, Adv. Atmos. Sci. (2018), doi:10.1007/s00376-017-7092-4.
[14] A. Mamun, Y. Chen, J. Liang, Radiative and cloud microphysical effects of the Saharan dust simulated by the WRF-Chem model, J. Atmos. Sol. Terr. Phys. 218 (2021) 105646, doi:10.1016/j.jastp.2021.105646.
[15] A. Oluleye, E.C. Okogbue, Analysis of temporal and spatial variability of total column ozone over West Africa using daily TOMS measurements, Atmos. Pollut. Res. (2013), doi:10.5094/apr.2013.044.
[16] J.H. Seinfeld, S.N. Pandis, Atmospheric Chemistry and Physics: From Air Pollution to Climate Change, 2nd edn., John Wiley & Sons, New York, 2006.
[17] S.A. Twomey, The influence of pollution on the shortwave albedo of clouds, J. Atmos. Sci. 34 (1977) 1149–1152 1977.
[18] P. Knippertz, Dust mobilization in the West African heat trough – the role of the diurnal cycle and of extratropical synoptic disturbances, Meteorologische Zeitschrift 17 (2008) 553–563.
[19] S. Engelstaedter, R. Washington, Atmospheric controls on the annual cycle of North African dust, J. Geophys. Res. Atmos. (2007), doi:10.1029/2006JD007195.
[20] F. De Longueville, Y.C. Hountondji, S. Henry, P. Ozer, What we do know about effects of desert dust on air quality and human in West Africa compared to other regions? Sci. Total. Environ. (2010), doi:10.1016/j.scitotenv.2010.09.025.
[21] C.D. Wells, M. Kasoar, M. Ezzati, A. Voulgarakis, Significant human health co-benefits of mitigating African emissions, Atmos. Chem. Phys. 24 (2024) 1025–1039, doi:10.5194/acp-24-1025-2024.
[22] S.M. Almeida, M. Manousakas, E. Diapouli, Z. Kertesz, L. Samek, E. Hristova, K. Sega, Padilla Alvarez, C.A. Belis, K. Eleftheriadis, Ambient particulate matter source apportionment using receptor modelling in European and Central Asia urban areas, Environ. Pollut. (2020), doi:10.1016/j.envpol.2020.115199.
[23] A. Anuforom, L. Akeh, P. Okeke, F. Opara, Inter-annual variability and long-term trend of UV-absorbing aerosols during Harmattan season in sub-Saharan West Africa, Atmos. Environ. (2007), doi:10.1016/j.atmosenv.2006,11.024.
[24] O.A. Falaiye, T.O. Aro, E.B. Babatunde, Inter-annual variation of aerosol optical depth at Ilorin (8° 32^{I}N, 4° 34^{I}E), a Central State of Nigeria, Zuma J. Pure App. Sci. 5 (2) (2003) 197–204 /.
[25] J.A. Akinyoola, A. Oluleye, I.E. Gbode, A comprehensive analysis of aerosol-induced radiative forcing and regional warming patterns in West Africa, Res. Sq. (2024), doi:10.21203/rs.3.rs-3853878/v1.
[26] Qi Ran, John Moore, Tianyun Dong, Shao- Yi Lee, Wenjie Dong, Statistical bias correction for CESM-simulate $PM_{2.5}$, Environ. Res. Commun. 5 (2023) (2023) 101001, doi:10.1088/2515-7620/acf917.
[27] V.E. Weli, G.C. Emenike, Atmospheric aerosol loading over the urban canopy of PortHarcourt City, Nigeria, Int. J. Environ. Poll. Res. 6 (2) (2018) 38–53 Published by www.eajournals.org .
[28] S. Ogunjo, O. Olaniyan, C.F. Olusegun, F. Kayode, D. Okoh, G. Jenkins, The role of meteorological variables and aerosols in the transmission of COVID-19 during Harmattan season, GeoHealth 6 (2) (2022) e2021GH000521, doi:10.1029/2021GH000521.